

## Modelling thermomechanical degradation of moulded electronic packages using physics-based digital twin

Inamdar, A.; van Soestbergen, M.; Mavinkurve, A.; van Driel, W.D.; Zhang, G.Q.

**DOI**

[10.1016/j.microrel.2024.115416](https://doi.org/10.1016/j.microrel.2024.115416)

**Publication date**

2024

**Document Version**

Final published version

**Published in**

Microelectronics Reliability

**Citation (APA)**

Inamdar, A., van Soestbergen, M., Mavinkurve, A., van Driel, W. D., & Zhang, G. Q. (2024). Modelling thermomechanical degradation of moulded electronic packages using physics-based digital twin. *Microelectronics Reliability*, 157, Article 115416. <https://doi.org/10.1016/j.microrel.2024.115416>

**Important note**

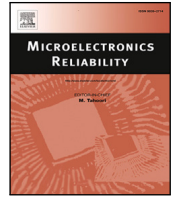
To cite this publication, please use the final published version (if applicable). Please check the document version above.

**Copyright**

Other than for strictly personal use, it is not permitted to download, forward or distribute the text or part of it, without the consent of the author(s) and/or copyright holder(s), unless the work is under an open content license such as Creative Commons.

**Takedown policy**

Please contact us and provide details if you believe this document breaches copyrights. We will remove access to the work immediately and investigate your claim.



## Research Paper

# Modelling thermomechanical degradation of moulded electronic packages using physics-based digital twin

A. Inamdar<sup>a,\*</sup>, M. van Soestbergen<sup>b</sup>, A. Mavinkurve<sup>b</sup>, W.D. van Driel<sup>a</sup>, G.Q. Zhang<sup>a</sup>

<sup>a</sup> Delft University of Technology, Mekelweg 5, 2628 CD, Delft, The Netherlands

<sup>b</sup> NXP Semiconductors, Gerstweg 2, 6534 AE, Nijmegen, The Netherlands

## ARTICLE INFO

## Keywords:

Physics of degradation  
Digital twin  
Epoxy moulding compounds  
Thermal ageing  
Package warpage

## ABSTRACT

Semiconductor devices are commonly encapsulated with Epoxy-based Moulding Compounds (EMC) to form an electronic package. EMC typically occupies a large volume within a package, and thus, governs its thermomechanical behaviour. When exposed to high temperatures (150 °C and above), electronic packages predominantly show oxidation of the outer layer of EMC. Oxidized EMC exhibits notably different material properties, resulting in a modified deformation pattern of a thermally aged package under varying thermal loads. As the oxidation layer grows in thickness, its mechanical properties also evolve, indicating distinct phases of the oxidized material at different stages of thermal ageing. Reflecting these changes (*i.e.*, the current state of degradation) into a Finite Element (FE) model-based analysis can provide better insights into failure prediction and component reliability. It requires updating the geometry and material behaviour as a function of ageing. This paper presents a systematic procedure to build a continuously updated physics-based Digital Twin of a thermally aged flip-chip package that can represent intermediate oxidation stages. First, experimental measurements are carried out to quantify the growth of the oxidation thickness at 150 °C and a diffusion-dominant mathematical model is proposed. Then, an accurate geometry of the test package is prepared with a parametric outer layer from all exposed sides of EMC to represent the oxidized layer at different stages of thermal ageing. Next, the experimental characterization of a few partially oxidized EMC specimens is done, and analytical methods are utilized to extract the thermomechanical properties of the oxidized EMC at different stages of ageing. Experimental warpage data of aged test packages are utilized to verify the defined material-model parameters that represent curing shrinkage, thermal expansion, glass transition, and corresponding elasticity moduli of the oxidized EMC at select stages of ageing. Then, a workflow to establish continuity in the material model is presented. Finally, the developed Digital Twin is utilized for an FE analysis to study the change in the trend of out-of-plane package deformations as a function of several stages of EMC oxidation.

## 1. Introduction

Electronic devices are being utilized in an increasing number of application fields such as manufacturing, automotive, and healthcare [1–3]. In some applications, electronic components are exposed to harsh environments such as elevated temperatures. To cover these application environments, the Automotive Electronic Council (AEC) defines standard qualification tests involving temperature variation between –40 °C and 125 °C, mechanical vibrations with a peak acceleration of 50 g, and humid environments up to 85% RH [4]. Under the operating loads, the constituent materials of an electronic component undergo degenerative changes over time, which are typically accelerated under harsh conditions. The term ‘*physics-of-degradation*’ encompasses the study of degradation mechanisms. It is closely linked with *physics-of-failure* since degradation leads to component failure. Thus, the reliability of an

electronic device is directly linked with the degenerative changes in its constituent materials.

Material degradation can be associated with one or more of the following five key domains — mechanical, thermal, chemical, electrical, and biological degradation. Among the dominant environmental loads (*viz.*, temperature, vibrations, humidity, and dust), exposure to high temperature is one of the biggest contributing factors for failures in electronic components [5]. To protect the electronic circuits from environmental loads, they are commonly encapsulated with thermosetting materials using a moulding process. Epoxy-based Moulding Compounds (EMC) are widely chosen for this purpose due to their desirable mechanical and chemical properties while being cost-effective [6–8]. Serving as a protective layer for the internal circuitry, the encapsulation material is, thus, most exposed to the environment. Therefore,

\* Corresponding author.

E-mail address: [a.s.inamdar-1@tudelft.nl](mailto:a.s.inamdar-1@tudelft.nl) (A. Inamdar).

<https://doi.org/10.1016/j.microrel.2024.115416>

Received 9 February 2024; Received in revised form 3 April 2024; Accepted 28 April 2024

Available online 13 May 2024

0026-2714/© 2024 The Author(s). Published by Elsevier Ltd. This is an open access article under the CC BY license (<http://creativecommons.org/licenses/by/4.0/>).

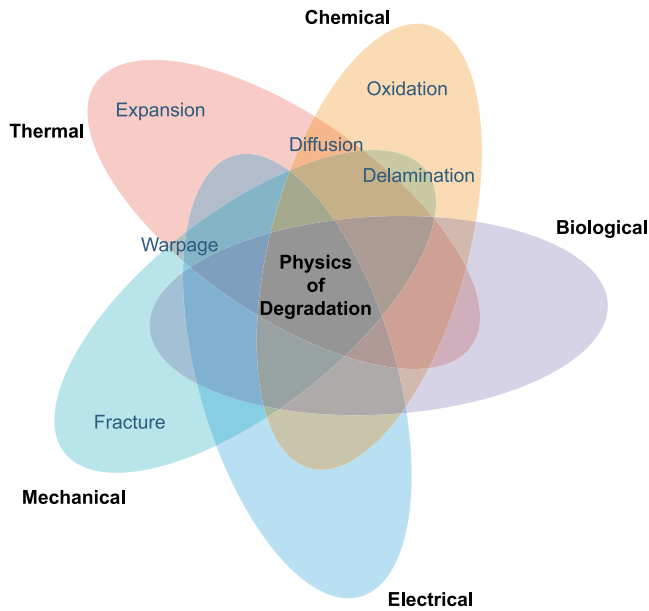


Fig. 1. The five domains of physics-of-degradation and a few ageing and failure mechanisms associated with the thermal–chemical–mechanical overlap.

ageing of EMC is one of the most important aspects of the ageing of electronic packages. Fig. 1 indicates the five domains of ageing along with a select number of degradation and failure mechanisms relevant to the scope of this article.

Thermal ageing of EMC results in the oxidation of its outer layer through its contact with atmospheric oxygen. It has been established with Fourier Transform Infrared (FT-IR) spectroscopy measurements that the ageing process changes the material chemically [9,10]. Moreover, the changes in thermomechanical properties of thermally aged EMC specimens have also been reported [11, ch.7], [12, ch.5]. Owing to its volume-share as high as 75% [13] within a typical electronic package, encapsulation tends to govern the overall mechanical behaviour of the electronic component [14]. Thus, degenerative changes in moulding compounds can significantly affect component lifetime.

Fig. 2 shows the cross sections of three thermally aged EMC specimens, oxidized at three different temperatures of 175 °C, 200 °C, and 225 °C for over 165 h, observed under a fluorescence microscope. Within a single specimen, the two different colours indicate two distinct ‘phases’ of EMC — pristine and oxidized. The colour gradient in Stage 1 shows a gradual transformation from an oxidized to a pristine phase, whereas Stage 3 indicates a clear distinction between these two phases. The difference in the colour composition of the oxidized layers across three different specimens highlights different ‘stages’ of EMC oxidation. It is crucial to identify the distinction in these stages while modelling the degradation phenomenon. As thermal ageing progresses, the oxidation layer grows in thickness, and the outer layer of EMC becomes more and more oxidized [15, pp. 68–74].

In general, the growth of oxidation thickness is both time- and temperature-dependent [16]. At higher temperatures, the oxidation layer grows faster, resulting in a darker layer that is easier to distinguish. At lower temperatures, the oxidation layer grows slower, and a prominent gradient from pristine to oxidized state is observed. The temperature dependency of the ageing process is presented in Refs. [12, pp. 73–76], [17,18], where the cross sections of thermally aged EMC specimens indicate that the same storage time at different ageing temperatures results in different stages of EMC oxidation.

In the current work, we focus on the time dependency of the ageing process carried out at a constant temperature of 150 °C. Therefore, different ageing stages correlate to different storage times. Fig. 3

illustrates three different stages of EMC oxidation obtained by isothermal ageing of bar-shaped EMC specimens with rectangular cross sections. Note the increased thickness and changed colour of the oxidized layer from left to right. The latter also indicates changes in material properties.

In the case of ageing of an encapsulated electronic package, the outer layer of EMC is oxidized to form an outer shell. It exhibits modified thermomechanical properties and modifies the mechanical behaviour of the entire package. This can accelerate certain failure modes, such as delamination along the EMC-die interface, cracks in the bulk of EMC [9], and fatigue failure of solder joints [19]. Thus, a virtual model of a microelectronic package that can capture these failure modes needs to incorporate the effect of ageing.

A Digital Twin-based modelling approach can be utilized to address this. This approach requires an active connection between the physical entity and its virtual representation for data and information exchange. This facilitates a continuous update of the virtual model to reflect the current state of the physical entity. In a physics-based approach, degenerative changes in a material are modelled using the physics-of-degradation. A physics-based Digital Twin can provide more insights on the effects of material degradation on different failure mechanisms, can facilitate prediction of component failure, and therefore, plays a key role in the Prognostics and Health Management (PHM) of electronics [20–22]. Thus, a dedicated physics-based Digital Twin model of an electronic component should reflect the changes in material composition (the extent of degradation) and material behaviour (the changes in the aged part of the component).

Here, the focus is on quantifying gradual degenerative changes within EMC, which can be achieved by representing the two aspects at any stage of thermal ageing – (a) the thickness of the oxidized layer and (b) its thermomechanical properties at the current stage. The first aspect has been addressed in some previous studies, which present the models for the growth of oxidation thickness using either physics-based laws or empirical relations based on activation energies [11, p. 133], [12, p. 74], [15, p. 72], [19].

The second aspect, however, is not well addressed in the literature. Thermomechanical properties of the oxidized EMC are, in most cases, determined at only one particular stage of EMC oxidation (e.g., 150 °C for 2000 h) [17]. This approach is insufficient as it does not provide any information about the intermediate stages of ageing. Moreover, the aforementioned FT-IR study [10] reports gradual chemical changes as a function of storage time for ageing up to 5000 h at 200 °C and 250 °C. Thus, thermomechanical properties of just one configuration of the oxidized EMC cannot simply be assumed the same and utilized throughout to represent any intermediate stage of thermal ageing. The current work in this article aims to address this gap.

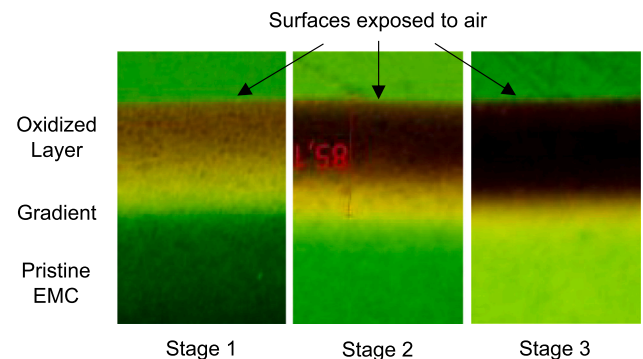


Fig. 2. Cross sections of EMC specimens, oxidized at three different temperatures of 175 °C, 200 °C, and 225 °C for over 165 h, observed under a fluorescence microscope. Each image represents a different ‘stage’ of ageing, while the distinct colours within each specimen indicate two different ‘phases’ of EMC — pristine and oxidized.

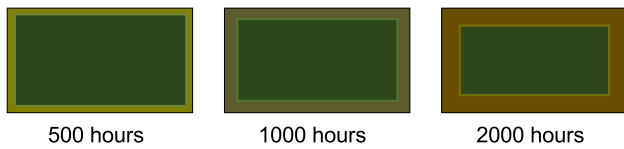


Fig. 3. A schematic representation of the rectangular cross sections of (partially oxidized) bar-shaped EMC specimens which are isothermally aged at 150 °C. The oxidation layer not only grows in thickness as a function of ageing time but also changes its colour from pale green to dark brown.

This article is organized into two main parts (and is an extended version of a previous conference paper [23]). The initial part focuses on preparing an experimentally validated physics-based Digital Twin, and the latter on using that for a simulation-based study. First, a systematic methodology is presented to prepare an experimentally validated physics-based Digital Twin, which can reflect the progress of degradation in an electronic package due to High-Temperature Storage (HTS). It consists of three steps – (i) quantifying the extent of degradation, (ii) preparing a parametric geometry of the Device Under Test (DUT), and (iii) obtaining an ageing-stage-dependent material behavioural model. These steps are described in Sections 2, 3, and 4.

Next, the prepared continuously updated package-degradation model is utilized to study the effect of EMC oxidation (using FE simulations) on the warpage of the DUT, *i.e.*, an electronic package. It focuses on two aspects — (1) the change in the maximum warpage of a thermally aged package (several ageing stages) at room temperature and (2) the change in the shape of the warpage curve under a thermal cycle in Sections 5 and 6, respectively. Finally, the simulation results are analysed in the context of failure prediction (solder fatigue and EMC-die delamination), underlining the contribution of a continuously updated Digital Twin in the PHM of electronics packaging and electronics-enabled systems.

## 2. Quantification of oxidation layer thickness

EMC oxidation is a combination of two simultaneous processes – (1) the diffusion of oxygen (from the surrounding air) into the free volume of the polymer network and (2) the chemical reaction of oxygen with the resin. Thus, it depends on the oxygen permeability of the material and the intrinsic rate of oxidation [16]. It results in a heterogeneous oxidized layer only up to a certain depth from the exposed surface because epoxies are fairly reactive but have low oxygen permeability [24]. Elevated temperatures facilitate a higher oxidation rate because of the higher activation energies [25], but the rate also slows down as the oxide thickness grows because it acts as a barrier for further diffusion of the atmospheric oxygen due to its increased density [12, pp. 73–76]. Thermo-oxidation of EMC is dominated by the diffusion of oxygen through the polymer [26] and is referred to as Diffusion-limited Oxidation (DLO).

In the case of thermal ageing at a constant temperature, the thickness of the resulting oxidation layer defines a particular ‘ageing stage’. To prepare a degradation model, the Thickness of the Oxidation Layer (TOL) was experimentally measured as a function of storage time ( $t$ ). Bar-shaped EMC specimens (80 mm × 10 mm × 4 mm) were thermally aged for up to 3000 h at 150 °C, which is above the glass transition temperature ( $T_g$ ) of the selected EMC. The aged (partially-oxidized) specimens were cross-sectioned and observed under a fluorescence microscope with ultraviolet (UV) illumination. The minimum and maximum value of the TOL was measured at multiple locations within each specimen by defining two boundaries — the first between the dark-brown and the yellow region and the second between the yellow and the green region (refer ‘Stage 1’ in Fig. 2 for the context). The mean value was utilized as the recorded TOL at different ageing times. Fig. 4 shows the measured data in red.

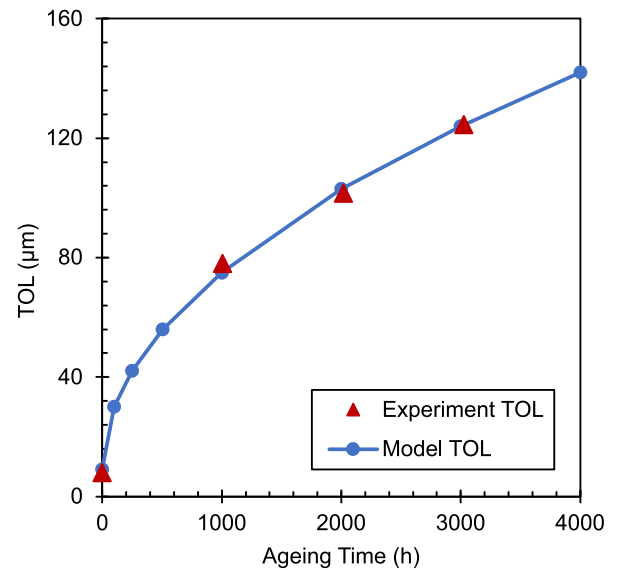


Fig. 4. Experimentally measured TOL data (red) for thermal ageing at 150 °C fitted to the ‘EMC Oxidation Model’, which follows the mathematical relation  $d = d_0 + d_1 t^n$ , where  $d$  is the oxidation layer thickness,  $t$  is the ageing time, and the rest are fitting parameters with values  $n = 0.5$ ,  $d_0 = 8.7 \mu\text{m}$ , and  $d_1 = 2.1 \mu\text{m}/\text{h}^n$ . TOL values generated using the model are indicated in blue.

The oxidation process, being diffusion-limited (*i.e.*, DLO), is often modelled as a diffusion-dominant process with a direct proportionality to the square root of time [15, pp. 68–74], *i.e.*,  $d \propto \sqrt{t}$ , where  $d$  is the TOL. The above relation was considered as the basis for the oxidation growth model. The proposed degradation model takes the form of Eq. (1), where  $d_0$ ,  $d_1$ , and  $n$  are fitting parameters. Instead of directly using the square root of time, a slightly more flexible version with  $n \in (0, 1)$  was used as a starting point.

$$d = d_0 + d_1 t^n \quad (1)$$

A standard curve fitting procedure was followed to determine the parameter values ( $d_0 = 8.7 \mu\text{m}$ ,  $d_1 = 2.1 \mu\text{m}/\text{h}^n$ , and  $n = 0.5$ ). A non-zero value of the parameter  $d_0$  reflects the oxidation thickness ( $\approx 9 \mu\text{m}$ ) at  $t = 0$  due to processes such as the Post Mould Cure (PMC) prior to the ageing experiment. Interestingly, the value deduced for the parameter  $n$  is exactly equal to 0.5. The oxidation growth model fitted to the experimental data is indicated in Fig. 4, along with some additional TOL values (marked blue) calculated using the finalized model. These values and associated material behaviour are utilized later in Sections 5 and 6.

## 3. Parametric geometry of test package

The second step is to create a geometric model of a test device such that it can be updated to reflect the current degradation state. A Ball Grid Array (BGA) package with a flip-chip construction (*i.e.*, die-substrate interconnects are copper pillars with solder caps) was chosen as the DUT. Initially, the geometry of a non-aged package was constructed, and then, some simplifications were incorporated to optimize for the required computational efforts. The substrate has a total of five layers (three metallization layers and two intermediate layers for copper vias), each of which was modelled individually as a homogenized layer. Layer-wise equivalent material properties were calculated by volume-based weighted averaging of the (linear elastic temperature-dependent) mechanical properties of copper and the utilized polymer. Moreover, the copper pillars and solder caps in the flip-chip construction were modelled in detail as cylindrical structures. For the chosen DUT, the EMC encapsulates only the die and

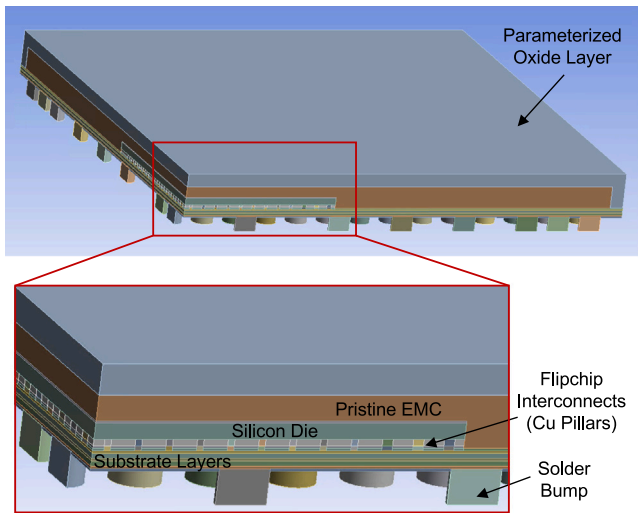


Fig. 5. The prepared quarter geometry of the thermally aged DUT (a flip-chip BGA package) with annotations for its sub-layers, including a parameterized outer layer for the oxidized EMC.

die-substrate interconnects (including the underfill) and rests on the substrate (*i.e.*, does not encapsulate the substrate).

To reflect the growth of the oxidation layer within EMC, a single parameter was defined to represent the current value of TOL. It was assumed that the oxidation layer grows uniformly in directions perpendicular to all exposed surfaces of the EMC, which is also a good representation of reality. This results in a core-shell structure representing two distinct layers of the EMC — oxidized and pristine. Fig. 5 indicates the core-shell style geometry of the thermally aged package. Considering symmetry, the required computational effort was reduced by using a quarter-geometry of the DUT.

A parametric setting was utilized along with an automation routine to update the geometric model using a variable TOL value representing any stages of EMC oxidation (isothermal at 150 °C) for up to 28 640 h ( $\approx 3$  years). The TOL growth beyond 3000 h is extrapolated using the fitted model. Appropriate settings were applied to maintain the mesh quality for all intermediate stages of ageing. This setting assumes there would be no cracking in the EMC, which could affect  $O_2$  diffusion into the bulk. Fig. 6 indicates the mesh in the two near-extreme cases within the range of oxidation. Higher-order finite elements (quadratic shape functions) with a mix of tetrahedral and hexahedral shapes and about 400 000 in number were utilized to ensure good quality results for all the considered cases. At any given ageing stage, the 'core' EMC would be assigned the 'pristine' material properties while the 'shell' (oxidized layer) gets the corresponding material properties of the oxidized EMC at the current degradation stage. A detailed procedure to derive these material properties at any intermediate stage is discussed in the following section.

#### 4. Material behaviour of oxidized EMC

The third and most crucial aspect of a physics-based Digital Twin is reflecting the changes in material behaviour at different ageing stages. To determine the change in thermomechanical properties as a function of the EMC oxidation state, partially-oxidized EMC specimens were utilized in experimental characterization. Then, an analytical approach was pursued to calculate the effective properties of only the oxidized layer.

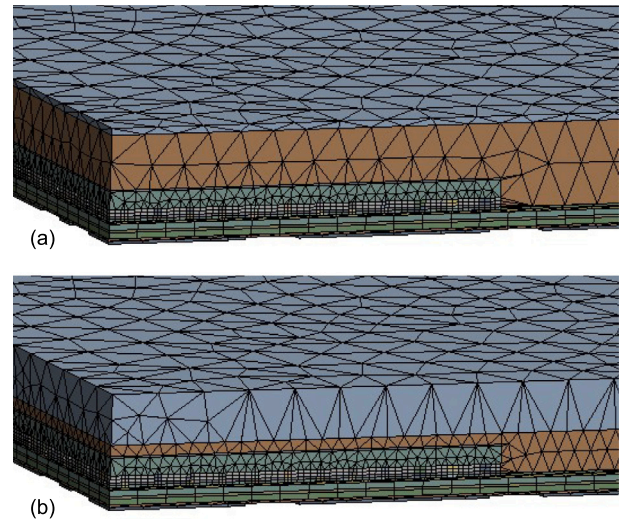


Fig. 6. The meshed package geometry of the two near-extreme cases within the range of EMC oxidation – (a) very thin (250 h, 42  $\mu\text{m}$ ) and (b) very thick (19 145 h, 300  $\mu\text{m}$ ) oxidized EMC layer. Quadratic finite elements are utilized to ensure good quality results for all the considered cases.

#### 4.1. Experimental characterization

Two different sets of bar-shaped EMC specimens with rectangular cross sections were thermally aged at 150 °C for 0 h, 500 h, 1000 h, 1500 h, 2000 h, 2500 h, and 3000 h. For each ageing stage, the modulus of elasticity ( $E$ ) was characterized using a single-frequency Dynamic Mechanical Analysis (DMA) at 1 Hz on the first set of aged specimens (80 mm  $\times$  10 mm  $\times$  4 mm); whereas the Coefficient of Thermal Expansion (CTE) and the shift in the glass transition temperature ( $T_g$ ) were characterized using Thermal-Mechanical Analysis (TMA) on the second set of thermally aged specimens (15 mm  $\times$  4 mm  $\times$  3 mm). In this way, the data of the linear elastic temperature-dependent material properties for the pristine (0 h aged specimens) and different partially-oxidized EMC specimens were gathered experimentally.

Note that this data does not indicate the behaviour of the oxidized EMC but that of an effective beam ( $E_{\text{eff}}$ ), which is a composite beam-like structure consisting of pristine EMC (core) and oxidized EMC (shell). Thus, the gathered data cannot directly be used for preparing the material model of the oxidized layer. Thus, analytical calculations were used for extracting the experimentally evaluated values for the oxidized EMC ( $E_{\text{ox}}$ ).

#### 4.2. Evaluation of elastic modulus

Elastic properties of the oxidized layer at each ageing configuration were derived from the experimental data using the flexural equation extended for multi-material composite beams. In this case, the cross-section of a partially-oxidized beam specimen consists of a 'core' pristine layer (thickness  $h_{\text{pr}}$ ) sandwiched between two 'shell' oxidized layers (thickness  $h_{\text{ox}}$  each). Fig. 7 illustrates the three-layer composite beam. Considering the wide aspect ratio of the cross section of beam specimens (*i.e.*, the width is over 2 times larger than the thickness), the analytical calculation considers the oxidation layer only on the top and bottom of the pristine layer with a common width  $b$ . Thus, the total beam thickness is  $h = h_{\text{pr}} + 2 h_{\text{ox}}$ .

The bending moment  $M$  is equated at a cross-section of an equivalent homogeneous beam with that of a composite beam and strain-continuity is applied across different layers of the beam cross-section. This is represented mathematically in Eq. (2); where  $\sigma$  is the axial stress (horizontal) on a differential cross-sectional area  $dA$  at a (vertical)

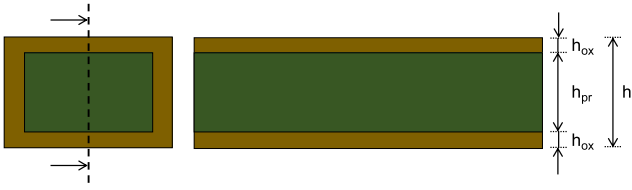


Fig. 7. The illustration of a partially oxidized bar-shaped EMC specimen with a rectangular cross-section as a three-layered composite beam with a total thickness ' $h$ '.  $h_{pr}$  is the thickness of the pristine EMC (core) while  $h_{ox}$  is that of the oxidized EMC layer (shell); and thus, follow the relation  $h = h_{pr} + 2h_{ox}$ .

distance  $y$  from the neutral axis of the beam,  $E$  is the elastic modulus, and  $\rho$  is the density.

$$M = \int_A \sigma y \, dA = \int_A \frac{E}{\rho} y^2 \, dA \quad (2)$$

Due to different elastic properties of pristine and oxidized layers, the stress  $\sigma$  is discontinuous, which splits the integral into two parts as shown in Eq. (3). The density is cancelled out from the integral because it remains practically unchanged, based on the internal tests for measuring the oxidation-induced shrinkage. Thus, the relation between effective elastic properties and that of individual layers boils down to Eq. (4), where  $E_{eff}$ ,  $E_{pr}$ ,  $E_{ox}$  are moduli of elasticity, and  $I_{eff}$ ,  $I_{pr}$ ,  $I_{ox}$  are the corresponding area moment of inertia, for the effective beam (partially-oxidized specimen), 'core' of the composite beam (pristine EMC), and 'shell' of the composite beam (oxidized EMC), respectively.

$$\int_{eff} \frac{E_{eff}}{\rho} y^2 \, dA = \int_{pr} \frac{E_{pr}}{\rho} y^2 \, dA + \int_{ox} \frac{E_{ox}}{\rho} y^2 \, dA \quad (3)$$

$$\Rightarrow E_{eff} I_{eff} = E_{pr} I_{pr} + E_{ox} I_{ox} \quad (4)$$

$$\Rightarrow E_{eff} h^3 = E_{pr} h_{pr}^3 + E_{ox} (h^3 - h_{pr}^3) \quad (5)$$

The principle of summing and subtracting the area moments of inertia to calculate values for composite cross-sections gives the expression  $I_{eff} = I_{pr} + I_{ox}$ . Utilizing the expressions  $I_{eff} = bh^3/12$ ,  $I_{pr} = bh_{pr}^3/12$  and the common width  $b$ , the equation gets further simplified to Eq. (5). Based on this, the values for  $E_{ox}$  at different ageing stages were evaluated using the linear elasticity data of  $E_{pr}$  and  $E_{eff}$ . Fig. 8 indicates the experimentally evaluated (ExpEval) values of  $E_{ox}$  from 20–300°C at three different stages of oxidation (blue, grey, and red dots).

#### 4.3. Mathematical model for elasticity

A mathematical model was fitted to the calculated elasticity data to obtain a smooth curve with an inverted S-shape. A few kernel functions were carefully considered to represent the temperature ( $T$ )-based relaxation of the modulus [27, ch.1]. Based on the comparison of their features such as being bounded and the point of 'symmetry' on a logarithmic scale (abscissa), the Kohlrausch–Williams–Watts (KWW) function was determined to be the most suitable empirical function. It is also referred to as the stretched exponential function and has a basic form given in Eq. (6), where  $a$  and  $b$  are scaling parameters. The KWW function is also widely used for representing relaxation phenomenon of various kinds, in particular, for amorphous materials such as polymers [28]. When resolved onto a linear scale (substituting  $T = \log(x)$ ), it takes the form of Eq. (7). Note that the common logarithm (base 10) is chosen here instead of the natural logarithm for a better fit to the experimentally obtained data.

$$f(x) = a \exp(-x^b) \quad (6)$$

$$\Rightarrow f(T) = a \exp(-10^{bT}) \quad (7)$$

The function was formulated such that it includes material parameters (*viz.*,  $E_g^{ox}$ ,  $E_r^{ox}$ ,  $T_g$ ) and incorporates temperature dependency. The

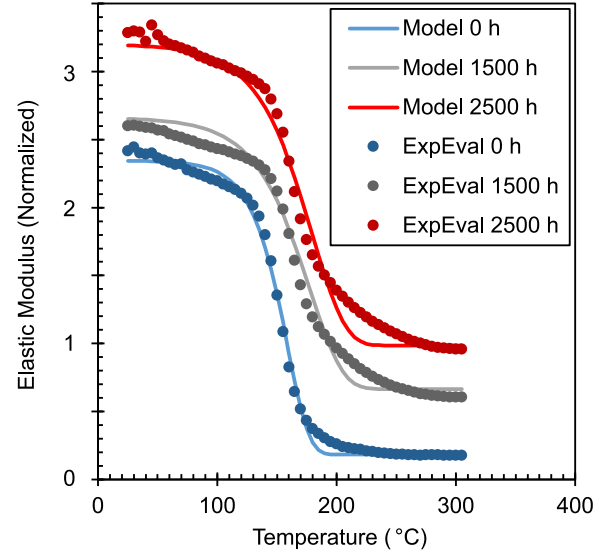


Fig. 8. Linear elastic temperature-dependent material model (Eq. (8)) fitted to the experimentally evaluated elasticity data  $E_{ox}$  (Section 4.2) of the oxidized EMC layer at three different stages of thermal ageing at 150°C.

final form of the adopted mathematical relation is given in Eq. (8). It essentially defines  $E_{ox}$  as a function of the temperature ( $T$ ); where  $f \in (0, 1)$ ,  $r$ , and  $s$  are fitting parameters;  $T_g^{ox}$  is the glass transition temperature;  $E_g^{ox}$  is the glassy modulus;  $E_r^{ox}$  is the rubbery modulus of the oxidized EMC at a particular ageing-stage.

$$E_{ox}(T) = E_r^{ox} + E_g^{ox} f \exp \left[ -10^{(T - T_g^{ox} - s)/r} \right] \quad (8)$$

Standard curve fitting techniques were utilized to obtain the values of the fitting parameters  $f$ ,  $r$ , and  $s$  at different ageing stages. For the pristine EMC, their values are  $f = 0.938$ ,  $r = 41.847$ , and  $s = 16.044$ ; whereas for all oxidized stages, they are  $f = 0.725$ ,  $r = 63.354$ , and  $s = 11.803$ . Fig. 8 shows the fit of the finalized material model (blue, grey, and red curves) to the experimentally evaluated  $E_{ox}$  data.

The proposed model allows obtaining elasticity curves for the oxidized EMC at any intermediate oxidation stage by determining just the values of three material-model parameters –  $T_g^{ox}$ ,  $E_g^{ox}$ , and  $E_r^{ox}$ . Thus, the parameterization of the material model is an important step in establishing continuity among different oxidation stages, more of which is described later in Section 4.6.

#### 4.4. Evaluation of CTE and $T_g$

A similar procedure was followed to evaluate the CTE and glass transition of the oxidized EMC. First, the experimental data of partially oxidized specimens were used to determine the  $\alpha_{eff}$  and  $T_g^{eff}$ . For each ageing stage, two straight lines were fit to the strain versus temperature data (TMA) using the standard curve fitting procedure. The slopes of these two lines were calculated for the  $\alpha_1^{eff}$  and  $\alpha_2^{eff}$  values; whereas the point of intersection of the two lines was used to obtain  $T_g^{eff}$ . Fig. 9 indicates an example of the described procedure for the 1000 h aged specimen.

Evaluating the CTE values of the oxidized EMC ( $\alpha_{ox}$ ) from  $\alpha_{eff}$  is not straightforward. The TMA test generally focuses on measuring only the change in the (dimension along the) length, while a bonded bi-material strip also shows a bending deformation due to a CTE mismatch between layers. Thus, the CTE calculation for a multi-material system requires more complex equations, including the moduli of elasticity of the involved layers. The relation between the thermal expansion-induced curvature of a bi-material strip and the properties ( $E$  and  $\alpha$ ) of its constituting materials is derived in the Ref. [29].

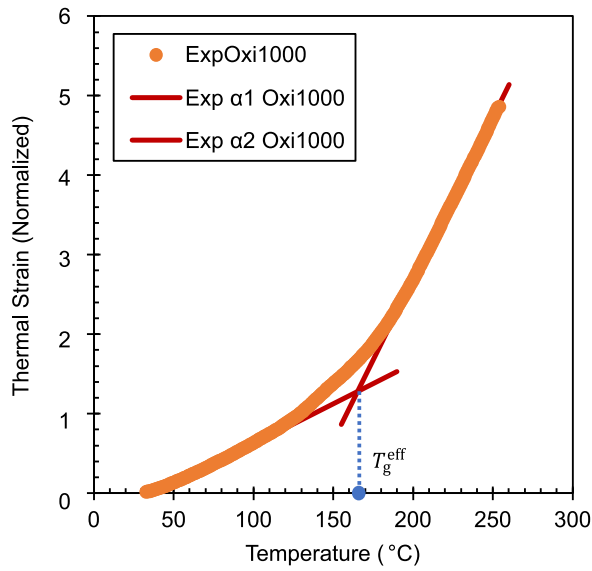


Fig. 9. Evaluation of the CTE values ( $\alpha_1^{\text{eff}}$  and  $\alpha_2^{\text{eff}}$ ) and the glass transition temperature  $T_g^{\text{eff}}$  of the partially-oxidized EMC specimen (aged at 150 °C for 1000 h) using the thermal strain vs. temperature data from TMA experiments.

However, the partially oxidized EMC specimens used here are symmetrically oxidized (from both the upper and lower surfaces of the beam). They are, therefore, expected to show negligible bending due to the CTE mismatch. Thus, available values of  $\alpha_{\text{pr}}$  and  $\alpha_{\text{eff}}$  from the TMA test results were utilized to calculate  $\alpha_{\text{ox}}$  at different ageing stages using volume-based weighted averaging, as indicated in Eq. (9). A similar approach has also been utilized in a previous publication [9]; however, this section provides much more context by elaborating on the reasoning behind implementing this method.

$$h \alpha_{\text{eff}} = h_{\text{pr}} \alpha_{\text{pr}} + (h - h_{\text{pr}}) \alpha_{\text{ox}} \quad (9)$$

The  $T_g$  is typically determined from the thermal strain versus temperature curves obtained from a TMA test. However, in this case, the  $T_g$  obtained from the TMA test would correspond to the partially-oxidized EMC specimen ( $T_g^{\text{eff}}$ ) and not to the oxidized layer ( $T_g^{\text{ox}}$ ). Thus, an additional ballpark value for  $T_g^{\text{ox}}$  of each oxidized stage was derived from the evaluated elastic modulus values ( $E_{\text{ox}}$  vs.  $T$ ) based on the DMA results (Fig. 8). Both values were treated as tentative  $T_g^{\text{ox}}$  values, which need further fine-tuning and verification.

In this way, the linear elastic thermomechanical behavioural model was obtained for the oxidized EMC at different stages of thermal ageing. The elasticity model relies on three parameters:  $T_g^{\text{ox}}$ ,  $E_{\text{g}}^{\text{ox}}$ , and  $E_{\text{r}}^{\text{ox}}$ ; whereas the tentative values of  $\alpha_{\text{ox}}$  and  $T_g^{\text{ox}}$  were also evaluated. Note that the above procedure provides only the initial estimates of the latter two. Thus, an experimental validation was carried out using the DUT to finalize the material model parameters.

#### 4.5. Experimental validation of material model

Experiments were designed around thermally aged DUT specimens to validate the material behavioural model. A few package specimens were stored at 150 °C for several ageing intervals of up to 3000 h. Then, the warpage of aged DUTs was measured at various temperatures between 25 °C (room temperature) and 260 °C. The specimens were exposed to high temperature at a rate of 60 °C/min in a controlled environment. In this context, the warpage indicates the out-of-plane deformation (along the Z-direction) measured on the top surface (XY plane) of the package.

A finite element simulation was set up on the parametric geometry of the DUT (Section 3) to reflect the experimental load conditions. A

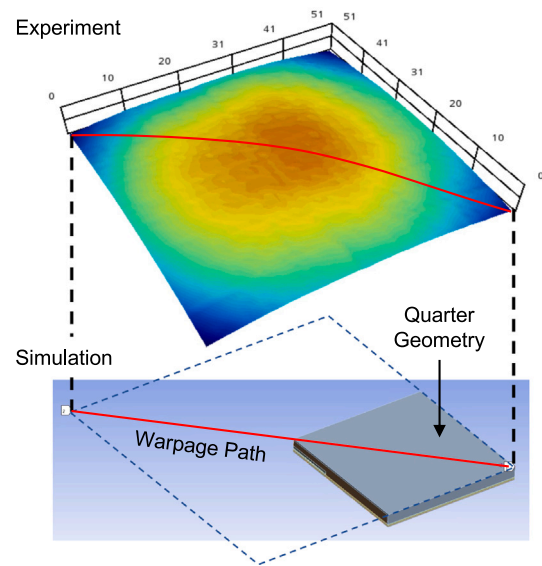


Fig. 10. Experimental validation of the material model (FE simulations) using warpage measurements along a diagonal path on the top surface of a thermally aged package. The spatial plot in the figure corresponds to the out-of-plane deformation at 100 °C of a package at the ageing stage of 1000 h.

diagonal path was defined along the top surface of the package, and the warpage along that path was extracted from the FE results. Fig. 10 shows the warpage evaluation path in the simulation and the experimental setting. The largest (in magnitude) out-of-plane deformation value along the diagonal path was recorded as the maximum warpage (Deformation Z) at several temperature values for comparison against the experimental data. Fig. 11 shows this comparison for the final validated model at three different ageing stages.

The warpage during a temperature variation primarily originates from the CTE-mismatch ( $\alpha$ ) among different layers of the package, which is further affected by the glass transition of EMC. Since the first utilized values of  $\alpha_{\text{ox}}$  and  $T_g^{\text{ox}}$  were just initial estimates (as described in Section 4.4), the initial simulation-based results showed a noticeable mismatch with the experimental trends. This Reason #1 was addressed by revising the two parameters  $\alpha_{\text{ox}}$  and  $T_g^{\text{ox}}$  in an iterative fashion within an acceptable range.

The Reason #2 behind this mismatch is the existence of an initial warpage and residual stresses due to the manufacturing process of a package, especially due to the moulding process. Residual stresses depend on several moulding conditions — packing/holding pressure, mould temperature, melt temperature, and injection velocity. A systematic experimental study of the effect of these parameters on the warpage of the moulded product has been presented in [30]. Several publications present characterization of warpage of the final product utilizing an analytical approach [31,32] or a FE-based numerical approach [33–37] with experimental validation.

Some studies describe the calculation of residual stresses after the moulding process (i.e., the state of ‘initial warpage’) using a viscoelastic temperature-dependent model. This initial warpage occurs due to two things – (i) the ‘cold shrinkage’ of all materials with a CTE mismatch among them, and (ii) the curing shrinkage of EMC during the moulding process. Both of these effects need to be coupled together for the FE simulation-based results to be closer to reality. Later, this ‘initial’ curing shrinkage is applied in finite element models using an initial-strain approach, in which the geometry is predefined with some initial strain values.

Moreover, viscoelastic properties of EMC are not only time and temperature-dependent but also vary based on the degree of cure (DOC) [34]. For composites such as moulding compounds, it has also

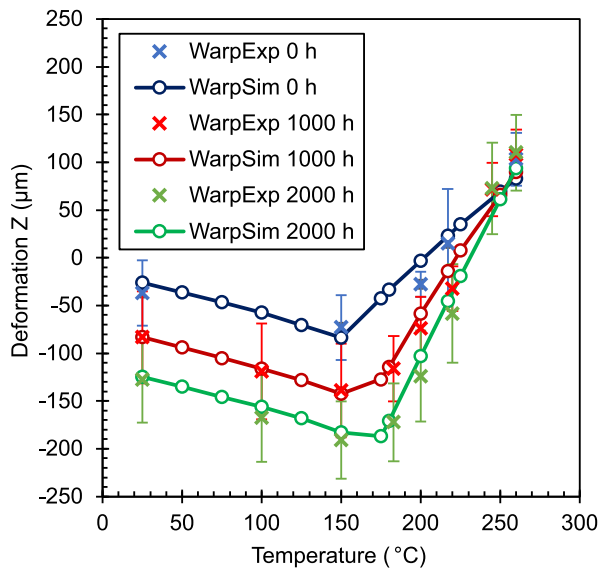


Fig. 11. The comparison of the experimental and FE-simulation data of the maximum warpage along the diagonal path (shown in Fig. 10) at different temperatures under a thermal load ramping from 25 °C (room temperature) to 260 °C at 60 °C/min. The negative warpage values indicate the direction of the deformation along the  $-z$  axis. The results show a good agreement between FE-simulation results (denoted by ‘o’) obtained using the finalized material model and the experimental data (denoted by ‘x’) of package specimens at three stages of thermal ageing – 0 h, 1000 h, and 2000 h.

been observed that lower filler content gives higher values of cure shrinkage [38, p. 40]. The shrinkage may or may not be linear with the DOC. A trend of non-linear change of thickness of epoxy resin specimens with respect to the DOC has been observed and modelled in an earlier publication [39]. The current study, however, assumes linear elastic (temperature-dependent) models for all materials, including the EMC. Thus, consideration of viscoelastic effects is out of the scope of this article.

The Reason #3 for the mismatch of experimental and simulation-based warpage results is the further curing shrinkage of EMC occurring after the moulding process (during PMC and later), which contributes to some additional warpage of the package. In general, during the curing process, the dimensional change occurs due to a combination of two processes — thermal expansion/contraction due to associated CTE (‘thermal shrinkage’) and chemical reaction (‘chemical shrinkage’). Thus, a coupling of thermo-chemical-mechanical modelling would be necessary to represent this, which is also out of the scope of the current study.

However, there exists another simpler way to address the aforementioned Reason #2 and Reason #3 and keep using the linear elastic temperature-dependent material models. Both the initial warpage and the curing shrinkage of EMC during moulding can be accounted for by adjusting its stress-free reference temperature ( $T_e$ ). Setting the  $T_e$  higher than  $T_{ref}$  of the entire geometry, when using linear elastic models, allows having the effect of initial strain and resulting additional deformation. Therefore, this technique was followed in this study to reflect the shrinkage in the FE simulation. The stress-free reference temperature of just the EMC material ( $T_e$ ) was assigned a value higher than the rest of the package. As a starting point, the stress-free reference temperature ( $T_{ref}$ ) of 180 °C was assigned to all components of the geometry, including the EMC. This was then updated by setting the  $T_e$  for pristine EMC to 190 °C.

It has also been reported that during thermo-oxidative changes, EMC undergoes additional shrinkage [40]. This was taken into account by setting the  $T_e$  of the oxidized EMC layer to an even higher value (>190 °C) than that of the pristine EMC. This was independently done for each ‘known’ oxidized stage of EMC. In this way, the material

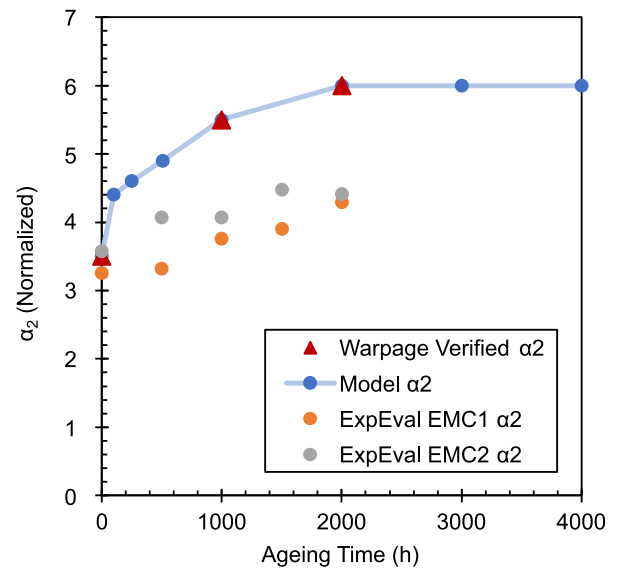


Fig. 12. The comparison of initial estimates (‘ExpEval’) of  $\alpha_2^{ox}$  with its values from the finalized material model (‘Warpage Verified’). Additional trend-based data points (blue) for interpolating the material-model parameter  $\alpha_2^{ox}$  are also indicated along with a trend line only indicative of continuity.

model parameters  $T_e^{ox}$ ,  $T_g^{ox}$ , and  $\alpha_2^{ox}$  (CTE after the glass transition) were updated over multiple iterations of FE simulations until a good match was found with experimental results (Fig. 11). Fig. 12 highlights the difference between the initial estimates (denoted by ‘ExpEval’) based on the procedure in Section 4.4 and the updated final values (denoted by ‘Warpage Verified’) of  $\alpha_2^{ox}$ .

#### 4.6. A continuous material model

With the prepared material model, the thermomechanical behaviour of the aged package can be simulated only at a select number of ageing stages. For obtaining the material behaviour of any other intermediate stage, the entire exercise of experimental data collection, analytical calculations, and simulation-driven validation-based parameter tuning must be carried out. However, there are practical limitations to the number of such ageing stages for which the entire cycle can be repeated. Therefore, it makes sense to interpolate the material behaviour for the intermediate ‘unknown’ stages based on the (validated material models at the) ‘known’ stages of ageing. This would essentially formulate a continuous material model for all stages of the oxidized EMC.

For this study, the continuity within EMC-oxidation stages was established by defining values for the material-model parameters (*viz.*,  $\alpha_1^{ox}$ ,  $\alpha_2^{ox}$ ,  $T_g^{ox}$ ,  $T_e^{ox}$ ,  $E_g^{ox}$ ,  $E_r^{ox}$ ) at additional intermediate ageing stages (here, ageing time  $t$ ). However, they cannot simply be linearly interpolated between two known stages. Each parameter shows a unique trend, especially in the early stages (0 h to 1000 h) of ageing. This was carefully considered for each of the material model parameters.

Overall, thermomechanical changes in the oxidized EMC tend to saturate beyond 2500–3000 h of ageing. Most material model parameters show a trend in three phases – (a) rapid initial growth, (b) slow increase, and (c) saturation. However, these three phases do not necessarily appear at the same ageing time ( $t$ ) for each parameter. Thus, additional information on the trends in the glass transition, shrinkage, and other aspects was sourced from the literature, and the intermediate values of the model parameters were defined accordingly at a select number of additional ageing stages (*viz.*, 100 h, 250 h, 505 h, and >3000 h).

For example, the experimental trends of EMC shrinkage during oxidation in Refs. [18,41] indicate a very sharp initial growth within

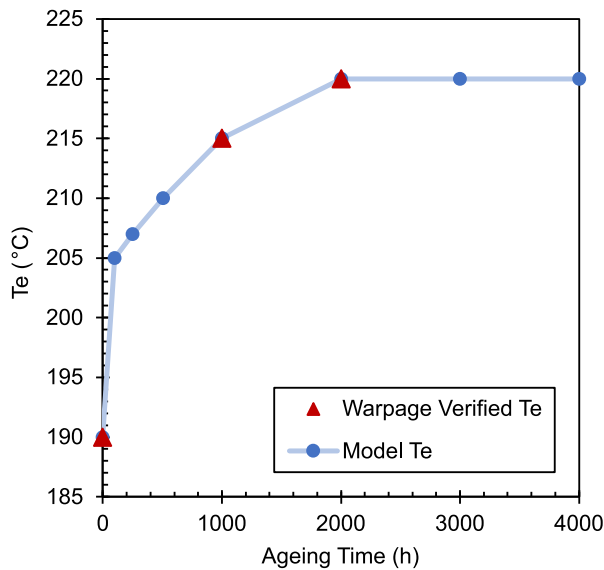


Fig. 13. Values of the material-model parameter  $T_e^{ox}$  at different ageing stages (trend line is only indicative of continuity). Experimentally verified values are marked in red, while the additional trend-based interpolated values are marked in blue.  $T_e^{ox}$  indicates the reference temperature (FE-simulations) of the oxidized EMC to account for the oxidation-induced shrinkage.

about 100 h of ageing followed by a near-constant saturation value. To reflect this shrinkage trend, additional data points for  $T_e^{ox}$  were created with a steep jump between 0 h and 100 h, and a more or less linear trend following the slope between 1000 h and 2000 h stages. Fig. 13 shows the development of  $T_e^{ox}$  as a function of ageing time. Red markers indicate values from the validated material models, while the trend-based intermediate values are marked in blue. A slightly modified trend was observed for the glass transition temperature  $T_g^{ox}$  [42] with the linear relation extending up to 3000 h. Fig. 14 shows the known (red) and additional (blue) intermediate  $T_g^{ox}$  values. In addition, it also highlights the disparity between the initial estimates (denoted by ‘ExpEval’) and warpage verified values from the finalized model.

The CTE before glass transition  $\alpha_1^{ox}$  stays nearly constant throughout the ageing time-domain (also observed in Ref. [12, pp. 86–90]), and thus, is represented with a constant function. It also remained unchanged from the initial estimates. The aforementioned generic trend was implemented for the additional data points of  $\alpha_2^{ox}$  by introducing an initial jump within the first 100 h of ageing and then a linear trend (Fig. 12).

Elasticity-related material parameters ( $E_g^{ox}$  and  $E_r^{ox}$ ) showed distinct trends. The glassy modulus stays nearly the same up to 1000 h of ageing but later shows a linear growth up to 3000 h. On the other hand, the rubbery modulus shows a more or less linear trend until 3000 h. A linear growth of  $E_r$  is also recorded in studies [42,43]. Fig. 15 shows  $E_r^{ox}$  as a function of ageing time, including the results evaluated from experimental characterization at different ageing stages.

The vertical shift in the elasticity curves for partially-oxidized EMC specimens (experimental data) tends to slow down and eventually saturate after a particular ageing time (also seen in the literature [44]). Since this change is essentially due to the changes in the oxidized layer, elasticity curves of the oxidized EMC were assumed to be constant above 3000 h of ageing. This is also the reason behind keeping the rest of the parameters constant beyond the 3000 h stage. Fig. 16 shows the linear elastic temperature-dependent elasticity model (storage modulus) for the oxidized EMC, including several intermediate stages between 0 h and 1000 h.

In this way, the additional values of material-model parameters at intermediate stages of EMC oxidation were introduced to form the basis

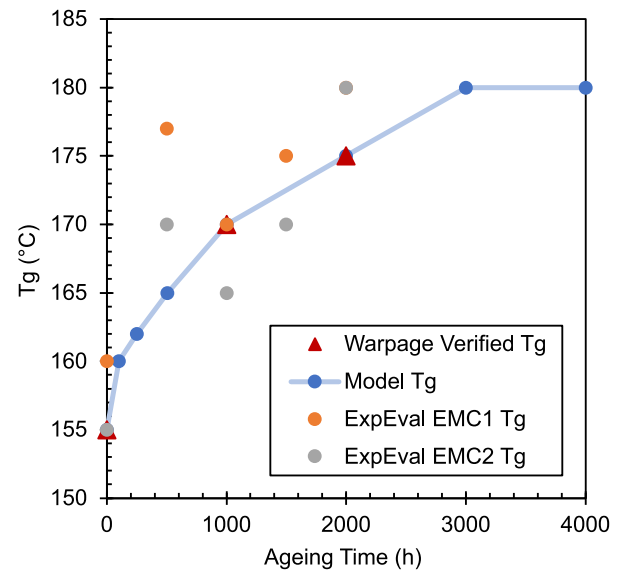


Fig. 14. The glass transition temperature of the oxidized EMC ( $T_g^{ox}$ ) at different ageing stages. The initial estimates (‘ExpEval’) show a nominal scatter around the experimentally verified values (red). Trend-based additional data points (blue) are connected with a trend line to indicate continuity.

of a continuous material model. All the graphs of these parameters (Figs. 12–16) show the data points joined with a trend line, which is only indicative of continuity. Each trend line is intentionally kept piecewise linear. A mathematical model is ideally required for each parameter –  $\alpha_1^{ox}$ ,  $\alpha_2^{ox}$ ,  $T_g^{ox}$ ,  $T_e^{ox}$ ,  $E_g^{ox}$ ,  $E_r^{ox}$  – to define a smooth curve indicating their dependency on ageing time ( $t$ ). However, this was deliberately not carried out owing to the fact that some of these points, although backed by the trends in the literature, are artificially interpolated. To create an even more robust continuous model, additional experimentally validated data points (i.e., more of the red triangles in the graphs) are required, especially in the first 1000 h of ageing.

The continuous material model reflects gradual changes in the thermomechanical behaviour of the oxidized EMC (Section 4). Combining this with the degradation model (Section 2) and package geometry (Section 3), a continuously updated physics-based Digital Twin capable of reflecting package-level thermomechanical degradation is achieved.

## 5. Maximum package-warpage at room temperature

Electronic packages, when exposed to a varying thermal load, exhibit warpage, i.e., a nonuniform out-of-plane deformation. Such a mechanical deformation results in additional stresses within several layers of a package and their interfaces. When applied in a cyclic fashion, it can lead to fatigue-based failure modes such as cracks in solder joints and EMC and the separation (delamination) at the interfaces of die-EMC, die-adhesive, adhesive-substrate, etc. Thus, warpage can serve as a good baseline indication to define the severity of failure modes.

Warpage due to thermal load originates from the difference in thermal expansion properties (CTE-mismatch) among the constitutive materials of a package. The glass transition of EMC is particularly crucial as it exhibits two different CTE values ( $\alpha_1^{pt}$ ,  $\alpha_2^{pt}$ ) leading to a sudden change in the deformation pattern in a short temperature range. A thermally aged package needs even more attention due to the presence of an additional layer of the oxidized EMC, which also exhibits a glass transition and two different CTE values ( $\alpha_1^{ox}$ ,  $\alpha_2^{ox}$ ). In addition, the relative difference in the elasticity of multiple layers also contributes to the resulting deformation pattern. Thus, the continuous material model of the prepared Digital Twin comes in particularly

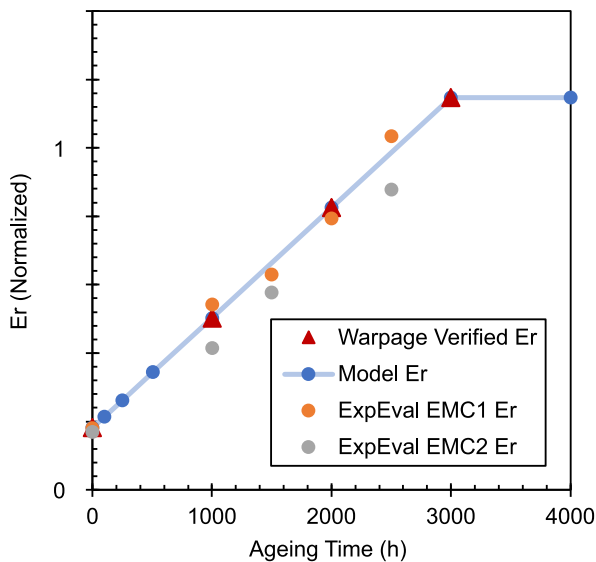


Fig. 15. The rubbery modulus of the oxidized EMC ( $E_r^{ox}$ ) as a function of ageing time. The experimentally evaluated values ('ExpEval') and the values from the elasticity model (Eq. (8)) show a close agreement and a linear growth trend up to 3000h of ageing is observed.

handy in determining the package warpage at any intermediate stage of thermal ageing.

This section analyses the effect of oxidation layer thickness on room temperature warpage. As described in Section 4.5, there exists inherent warpage at room temperature due to the manufacturing process (including moulding and solder reflow), which introduces a different 'stress-free temperature' (much higher than room temperature) for different materials. A finite element simulation was set up using the test-package geometry and prepared material model to evaluate the package warpage at room temperature under a uniform thermal load from 180 °C to 25 °C. In addition to the warpage-validated 'known' ageing stages – 0h, 1000h, 2000h, 3000h, three intermediate stages of 100h, 250h, and 505h were utilized. The TOL and material-model parameters for these intermediate stages are indicated in Figs. 4 and 12–16, respectively. The TOL values beyond 3000h were extrapolated using the same growth model, assuming it continues to follow the same trend. For the material properties at ageing stages beyond 3000h, appropriate assumptions described in Section 4.6 were followed.

It is important to note that the automated geometry update could be implemented up to 365  $\mu\text{m}$  of TOL (corresponding to 28 640h) since that is also the thickness of the EMC layer above the die. Beyond that, the geometry was manually updated by further expanding the EMC oxidation layer (from the top) only in the region around the die and also uniformly from the sides of the package. Finally, a theoretically plausible stage with a fully oxidized EMC layer corresponding to 62 500h (about 7 years) of isothermal ageing was also considered for the sake of comparison. The maximum value (by magnitude) of the out-of-plane deformation along the diagonal path (Fig. 10) was recorded at each considered aged state. Fig. 17 shows the simulation-based values as a function of TOL. For additional context, previously recorded experimental values are also indicated with error bars corresponding to  $\pm 3\sigma$ , where  $\sigma$  is the standard deviation. Experimental TOL values correspond to 0h, 1000h, and 2000h of ageing. Negative warpage values only indicate the direction of the deformation along the  $-z$  axis.

A rapid increase in the magnitude of maximum warpage is observed within the first 2000h of ageing (TOL  $\sim 100\mu\text{m}$ ). Then, the rate slows down drastically with respect to the ageing time ( $t$ ) until the TOL reaches 250  $\mu\text{m}$  (13 135h  $\approx 1.5$  years). Later, a saturation is seen near 350  $\mu\text{m}$  of TOL, and the curve reverses its trend after TOL 365  $\mu\text{m}$

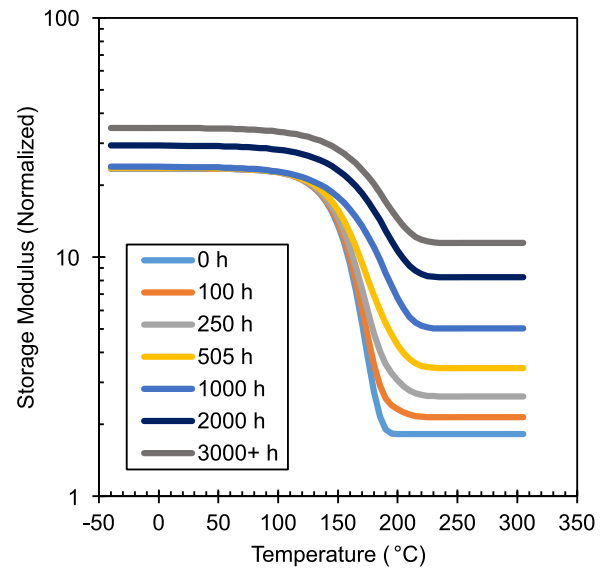


Fig. 16. The plots of linear elastic temperature-dependent elastic (storage) modulus of the oxidized EMC ( $E_{ox}$ ) for a few 'known' ageing stages, viz., 0h, 1000h, 2000h, and 3000h. Some additional plots for ageing stages between 0h and 1000h and beyond 3000h are also indicated based on the continuity of material-model parameters  $E_g^{ox}$ ,  $E_r^{ox}$ , and  $T_g^{ox}$ .

showing lower values (magnitude) of maximum warpage for all stages until the fully-oxidized stage. This interesting change can be explained by a combination of factors.

The TOL value and intermaterial interactions are the key contributing factors here because the material-model parameters are kept unchanged after the 3000h stage (TOL 365  $\mu\text{m}$ ). Note that the 'point of reversal' is the instance where the EMC right above the die is completely oxidized (refer Fig. 6 for context), which means, from this point onwards, the fully oxidized EMC (stiff) interacts directly with the silicon die (even stiffer) without any pristine EMC (softer) sandwiched between them. This pivotal point also marks about 75% of the total EMC volume being oxidized (i.e.,  $\sim 7\text{mm}^3$  pristine and  $\sim 18\text{mm}^3$  oxidized EMC). CTE does not seem to play a significant role in this phenomenon for three reasons – (1)  $\alpha_1^{ox}$  remains unchanged from  $\alpha_1^{pr}$ , (2)  $\alpha_2^{ox}$  does not play any role for the considered temperature range, i.e., thermal load, and (3)  $\alpha^{Si}$  remains nearly constant within a small range of 2.5–3.5 ppm/°C for the defined thermal load. Therefore, we conclude that the observed 'reversal' phenomenon is initiated and dominated by the direct interaction of two stiff materials (oxidized EMC and silicon die) in combination with a significantly high volume percentage ( $\geq 75\%$ ) of the oxidized layer within EMC.

## 6. Change in warpage curvature under thermal cycling

This section focuses on studying the changes in the package warpage induced by a thermal cyclic load as a function of EMC oxidation. A finite element simulation was set up with a thermal load including a single cycle from 25 °C to 260 °C with a 1 °C/sec heating and cooling ramp and an intermediate dwell time of 30 min at the highest temperature. The exercise was repeated for the same 17 ageing stages as in Section 5 (from pristine to fully oxidized), and the prepared continuous material model was utilized. The warpage was evaluated along the half of the path shown in Fig. 10, i.e., from one corner to the centre of the package. For the comparison at various temperature steps, the plots for relative deformation were created by setting the displacement at the 'package corner' end of the warpage path as zero. Figs. 18 and 21 show a few results. The numbers on the  $x$ -axis only indicate the relative position of the points along the warpage evaluation path, where '0' is the corner of the test package and '10' is its centre.

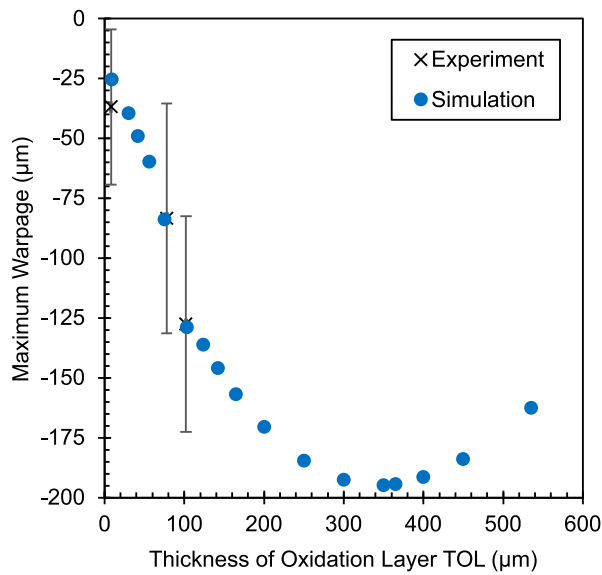


Fig. 17. Maximum warpage of the test package evaluated along the diagonal path (Fig. 10) as a function of oxidation layer thickness. The error bars of the experimental data correspond to  $\pm 3\sigma$ , where  $\sigma$  is the standard deviation.

The results at all ageing stages (Fig. 21) indicate one common trend: the reversal of the shape of the warpage curve from ‘smiling’ (–) to ‘frowning’ (–). There are two key aspects of this change – (i) the point (temperature step) at which the curvature reversal begins, and (ii) the actual point where the shape changes. Both of these aspects are primarily governed by the increasing volume share and evolving material properties of the oxidized EMC layer.

Fig. 18 shows the warpage graphs for the package without ageing. The beginning of the curvature change is observed at around 150 °C. This ‘pivot temperature’ shifts to higher temperature values as the oxidation stages progress. This can be seen in Fig. 21, where the plots in subfigures (a), (b), and (c) show the warpage curve at 180 °C higher than that of 150 °C (indicating the beginning of reversal), while the plot in subfigure (d) indicates the opposite. This means the pivot temperature moves from around 150 °C for the non-aged condition to beyond 180 °C for the 3000 h ageing stage.

This can be explained by the relative differences in the thermomechanical properties of various materials at a particular temperature. Figs. 19 and 20 show the elastic modulus and CTE of a few materials constituting various layers of the test package. The glass transition of EMC (pristine and oxidized) and the softening of solder material (due to the approaching melting point) occurs around the 150 °C mark. The softened layers allow the relaxation of inter-layer stresses and thus produce a less severely deformed shape of the warpage curve. This is further facilitated by a small CTE difference between EMC and most other materials (only a select few are shown in Fig. 20) in the glass transition region. The gradual shift of the pivot temperature can be explained by the gradual increase of  $T_g^{ox}$  for the higher stages of oxidation and the increasing volume share of the oxidized EMC. A polymer-dominant layer of the package substrate (named ‘CoreVia23’) was also considered for the comparison. The transition of that layer into softer material is relatively subtle and does not seem to affect the warpage change as much as the EMC does.

Fig. 21 shows the gradual shift of the actual ‘shape reversal temperature’ as a function of ageing. This value is between 200–217 °C for the non-aged stage (subfigure (a)), between 217–225 °C for the 1000 h stage (subfigure (b)), and between 225–250 °C for the 2000 h and 3000 h stages (subfigures (c) and (d)). Such a shift to higher values (temperature-delay) is expected to be caused by a combination of three things – (i) the increase in the volume percentage of the oxidized EMC, (ii) the

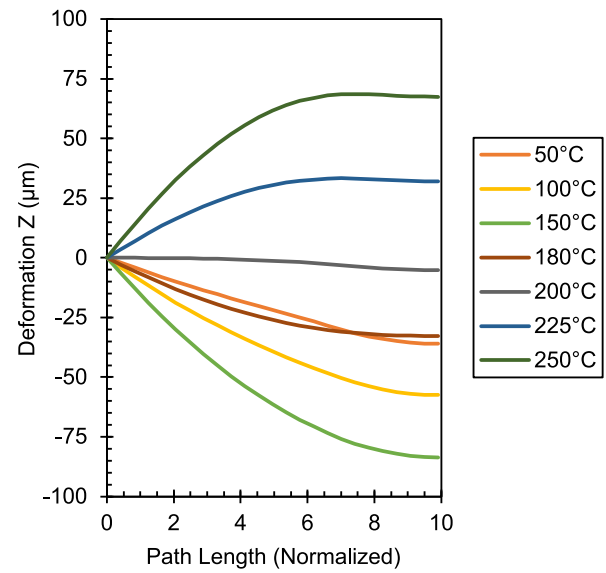


Fig. 18. Warpage curves of a pristine package (0h ageing) under a thermal cycle from 25 °C to 260 °C. The x-axis indicates the relative position of points along the warpage evaluation path, ‘0’ being the package corner and ‘10’ the centre. The shape of the curve begins to change the trend at around 150 °C and completely reverses from ‘smiling’ (–) to ‘frowning’ (–) beyond 200 °C.

increase in the value of  $T_e^{ox}$  (the stress-free temperature of the oxidized layer accounting for shrinkage), and (iii) the gradual shift of the glass transition region.

The results in the last two sections show that the EMC oxidation affects the package warpage at room temperature as well as its deformation behaviour under a varying thermal load. These changes are dominated by both the increase in the EMC oxidation thickness and the evolution of its material properties. The ‘current’ stage of the oxidized layer influences the warpage variation of a package under a thermal cyclic load. This, in turn, changes the accumulated damage in solder joints and affects the time to failure. Similarly, a differently warped package induces different stresses on the relatively stiff silicon die. This facilitates the delamination of the die-EMC interface. This can be observed by simulating solder fatigue and accrued damage at the die-corner. However, the analysis of such simulation results is out of the scope of this article and would be discussed in a future publication. Therefore, an experimentally validated physics-based Digital Twin can reflect the degradation more accurately and help visualize and predict the package behaviour and its impact on the associated failure modes.

## 7. Conclusion and outlook

Thermo-oxidative changes in moulding compounds modify the mechanical behaviour of an encapsulated electronic package. Reliability prediction can be enhanced by reflecting these changes in the finite element models. A physics-based Digital Twin, which is a continuously updated model, can reflect any state of degradation by updating the component geometry to the extent of degradation (quantified TOL) and material behaviour of the aged part of the component (oxidized EMC layer).

In particular, characterizing the material behaviour of only the oxidized EMC layer at different ageing stages is tricky. Thus, a hybrid approach was designed and implemented using experimental data, analytical calculations, and numerical validation to obtain six material model parameters:  $\alpha_1^{ox}$ ,  $\alpha_2^{ox}$ ,  $T_g^{ox}$ ,  $T_e^{ox}$ ,  $E_g^{ox}$ ,  $E_r^{ox}$ . This exercise also helps highlight the scope for further improvement by identifying where the

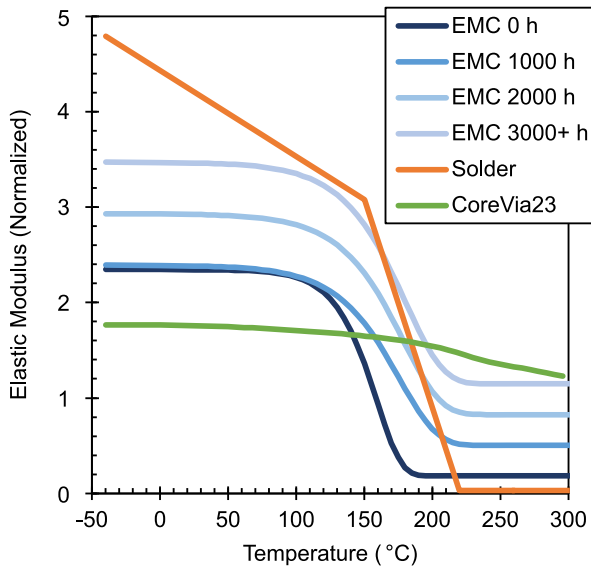


Fig. 19. The comparison of modulus of elasticity ( $E$ ) of several interacting layers within the test package, including a few stages of oxidized EMC. The softening of solder material beyond 150 °C and the glass transition of EMC in the range 150–200 °C contributes to the shape-change of warpage curves.

need for additional data collection is. Including more stages in the first 1000h of ageing to establish continuity in the material-model parameters can make the existing model even more robust.

The finite element simulations (Sections 5 and 6) show the changes in the package warpage as a function of ageing stages and indicate a heavy influence of the oxidized layer on the mechanical behaviour of the package. Thermal ageing increases the magnitude of the maximum warpage at room temperature up to the point when the EMC on top of the silicon die is completely oxidized and later decreases until the point of full oxidation.

In addition, thermally aged stages exhibit the change in the shape of the package warpage from ‘smiling’ (–) to ‘frowning’ (–) with a ‘temperature-delay’, *i.e.*, at a higher temperature compared to that of the pristine stage. This clearly indicates that failure predictions based on the FE models would vary depending on the ‘current’ state of oxidation. It also underlines the key role of incorporating a Digital Twin for the PHM of electronic components and systems.

The established workflow in this paper (Sections 2 to 4) can form the basis for the next step in modelling thermomechanical degradation of EMC. A more complex viscoelastic material model could be prepared, which would require additional model-parameters, a much larger design of experiments, and more intricate numerical simulations that can reflect viscoelastic effects.

The current study represents the oxidation layer by a single value, *i.e.*, TOL. The oxidized EMC layer can be represented with multiple sub-layers, each with a varying degree of oxidation from 100% oxidized to 0% (pristine) and the intermediate layers accounting for ‘diffused but unreacted  $O_2$ ’. This approach would require a more complex DoE and extensive FT-IR spectroscopy measurements.

Finally, the prepared physics-based Digital Twin can be used to study additional aspects and extract even more data, such as the die-level stresses, to study the effect on different package- and board-level mechanical failure modes and to develop a data-driven approach for failure prediction.

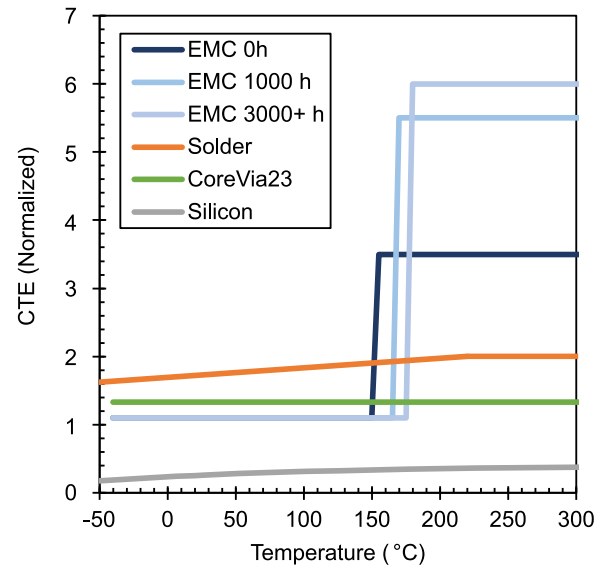


Fig. 20. The comparison of the coefficient of thermal expansion ( $\alpha$ ), of several materials constituting the test package. In addition to the gradual shift of  $T_g^{ox}$ , the  $\alpha_g^{ox}$  attains much higher values as a function of ageing, increasing the CTE mismatch with other materials even further in the rubbery phase of EMC.

#### CRedit authorship contribution statement

**A. Inamdar:** Conceptualization, Methodology, Formal analysis, Investigation, Writing – original draft, Visualization. **M. van Soestbergen:** Conceptualization, Methodology, Writing – review & editing, Supervision. **A. Mavinkurve:** Conceptualization, Methodology, Formal analysis, Resources, Project administration. **W.D. van Driel:** Supervision, Project administration, Funding acquisition. **G.Q. Zhang:** Supervision, Funding acquisition.

#### Declaration of competing interest

The authors declare that they have no known competing financial interests or personal relationships that could have appeared to influence the work reported in this paper.

#### Data availability

The data that has been used is confidential.

#### Acknowledgement

This work has been carried out within the *ArchitectECA2030* project under the grant agreement №877539. The project is co-funded by grants from Germany, Netherlands, Czech Republic, Austria, Norway, and Key Digital Technologies Joint Undertaking (*KDT JU*), formerly known as Electronic Component Systems for European Leadership Joint Undertaking (*ECSEL JU*).

The authors would also like to acknowledge Sumitomo Bakelite for providing test specimens and helping in thermal ageing, conducting thermomechanical analysis and further characterization. Furthermore, we are grateful to our colleagues L. Goumans (NXP Nijmegen) and C.S. Foong (NXP Austin) for their help in measuring the oxidation thickness using fluorescence microscopy and collecting the package warpage data.

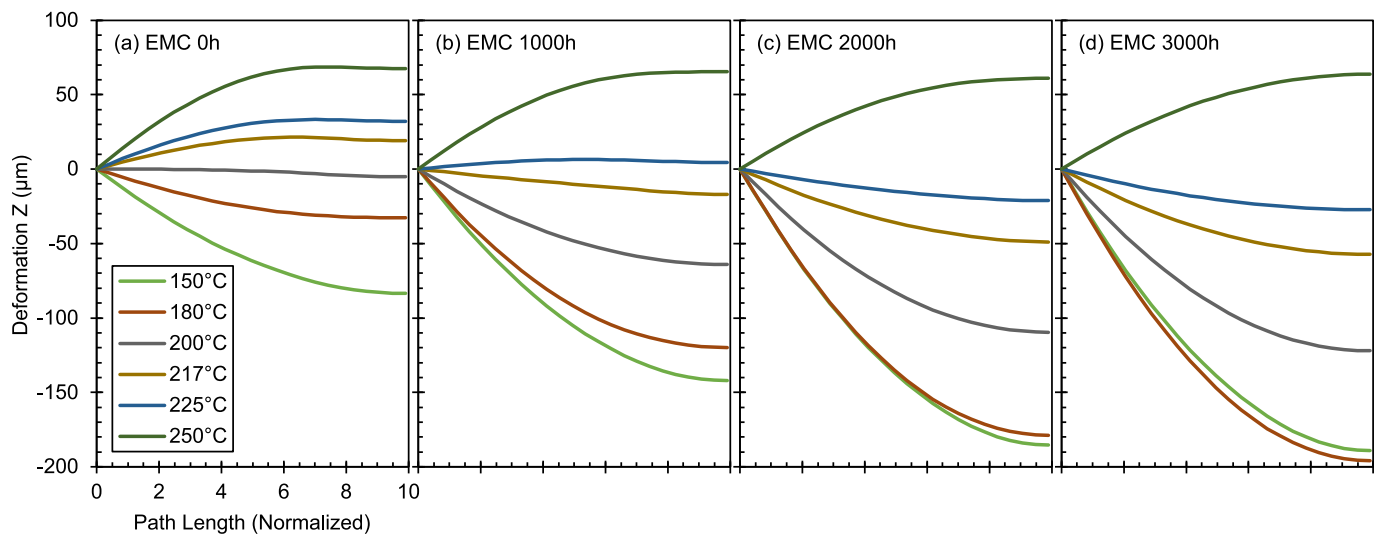


Fig. 21. The comparison of warpage curves of the test package (under a thermal cycle from 25 °C to 260 °C) at its four different stages of thermal ageing. The 'pivot temperature', where the shape of the warpage curve reverses the trend of change, shifts from around 150 °C (0h) to around 180 °C (3000h). Similarly, the 'shape reversal temperature' also attains higher values from between 200–217 °C (0h) to between 225–250 °C (2000h and 3000h) as a function of thermal ageing.

## References

- [1] S. Segars, Arm partners have shipped 200 billion chips, 2021, URL: <https://www.arm.com/blogs/blueprint/200bn-arm-chips>.
- [2] Yole Intelligence, Semiconductor trends in automotive 2022, 2022, URL: <https://www.yolegroup.com/product/report/semiconductor-trends-in-automotive-2022/>.
- [3] Precedence Research, Medical electronics market size to hit USD 248.43 billion, 2021, URL: <https://www.precedenceresearch.com/medical-electronics-market>.
- [4] AEC-Q100-Rev-H failure mechanism based stress test qualification for integrated circuits component technical committee automotive electronics council, 2014, URL: [http://www.aecouncil.com/Documents/AEC\\_Q100\\_Rev\\_H\\_Base\\_Document.pdf](http://www.aecouncil.com/Documents/AEC_Q100_Rev_H_Base_Document.pdf).
- [5] R.C. Chu, R.E. Simons, M. Iyengar, L.-T. Yeh, Thermal management of flip chip packages, in: Tong Ho-Ming, Lai Yi-Shao, C.P. Wong (Eds.), *Advanced Flip Chip Packaging*, volume 9781441957, Springer, Boston, MA, 2013, pp. 413–469, [http://dx.doi.org/10.1007/978-1-4419-5768-9\\_9](http://dx.doi.org/10.1007/978-1-4419-5768-9_9), URL: [https://link.springer.com/chapter/10.1007/978-1-4419-5768-9\\_9](https://link.springer.com/chapter/10.1007/978-1-4419-5768-9_9).
- [6] M.J. Mullins, D. Liu, H.J. Sue, Mechanical properties of thermosets, in: Q. Guo (Ed.), *Thermosets: Structure, Properties and Applications*, Woodhead Publishing, 2012, pp. 28–61, <http://dx.doi.org/10.1533/9780857097637.1.28>.
- [7] D. Carolan, A. Ivankovic, A.J. Kinloch, S. Sprenger, A.C. Taylor, Toughening of epoxy-based hybrid nanocomposites, *Polymer* 97 (2016) 179–190, <http://dx.doi.org/10.1016/J.POLYMER.2016.05.007>.
- [8] H. Ardebili, Jiawei Zhang, M.G. Pecht, Encapsulation technologies for electronic applications, *Encapsulation Technologies for Electronic Applications*, second ed., Elsevier, 2018, pp. 1–498, <http://dx.doi.org/10.1016/C2016-0-01829-6>.
- [9] A. Mavinkurve, L. Goumans, J. Martens, Epoxy molding compounds for high temperature applications, in: 2013 European Microelectronics Packaging Conference, EMPC, 2013, pp. 1–7, URL: <https://ieeexplore.ieee.org/document/6698694>.
- [10] P. Lall, S. Deshpande, Y. Luo, M. Bozack, L. Nguyen, M. Murtuza, Degradation mechanisms in electronic mold compounds subjected to high temperature in neighborhood of 200 °C, in: *Proceedings - Electronic Components and Technology Conference*, Institute of Electrical and Electronics Engineers Inc., 2014, pp. 242–254, <http://dx.doi.org/10.1109/ECTC.2014.6897295>.
- [11] J. De Vreugd, The effect of aging on molding compound properties (Ph.D. thesis), Delft University of Technology, 2011, URL: <https://repository.tudelft.nl/islandora/object/uuid%3A906aa318-3878-4183-ac11-f0f33eae34dd>.
- [12] B. Zhang, Material Characterization, Modelling and Simulation of Epoxy Moulding Compounds under High Temperature Storage and Temperature Cycling Thermal Ageing (Ph.D. thesis), Universität der Bundeswehr München, 2020, URL: <https://athene-forschung.unibw.de/doc/137120/137120.pdf>.
- [13] Y. Liu, *Power electronic packaging*, Power Electronic Packaging, Springer New York, 2012, <http://dx.doi.org/10.1007/978-1-4614-1053-9>.
- [14] S.P. Phansalkar, C. Kim, B. Han, Effect of critical properties of epoxy molding compound on warpage prediction: A critical review, *Microelectron. Reliab.* 130 (2022) 114480, <http://dx.doi.org/10.1016/J.MICROREL.2022.114480>.
- [15] E. Nguengang, *Experimental and Simulation-based Investigations on the Influence of Thermal Aging and Humidity on the Warpage of Molded Plastic Packages* (Ph.D. thesis), University of Stuttgart, 2013.
- [16] A. Quintana, M.C. Celina, Overview of DLO modeling and approaches to predict heterogeneous oxidative polymer degradation, *Polym. Degrad. Stab.* 149 (2018) 173–191, <http://dx.doi.org/10.1016/j.polymdegradstab.2017.11.014>.
- [17] A. Inamdar, Y.-H. Yang, A. Prisacaru, P. Gromala, B. Han, High temperature aging of epoxy-based molding compound and its effect on mechanical behavior of molded electronic package, *Polym. Degrad. Stab.* 188 (2021) <http://dx.doi.org/10.1016/j.polymdegradstab.2021.109572>.
- [18] L. Grandi, M. Rovitto, Thermal aging on molding compounds: Material characterization and modeling, in: 2022 23rd International Conference on Thermal, Mechanical and Multi-Physics Simulation and Experiments in Microelectronics and Microsystems, EuroSimE 2022, Institute of Electrical and Electronics Engineers Inc., 2022, <http://dx.doi.org/10.1109/EUROSIME54907.2022.9758856>.
- [19] A. Inamdar, P. Gromala, A. Prisacaru, A. Kabakchiev, Y. Yang, B. Han, EMC oxidation under high-temperature aging, in: W. van Driel, M. Mehr (Eds.), *Reliability of Organic Compounds in Microelectronics and Optoelectronics*, Springer, Cham, 2022, pp. 53–80, [http://dx.doi.org/10.1007/978-3-030-81576-9\\_3](http://dx.doi.org/10.1007/978-3-030-81576-9_3).
- [20] A. Inamdar, P. Gromala, W.D. van Driel, G.Q. Zhang, Making the digital twin work for mission critical electronics, *IEEE EPS Newsl.* July 2022 (2022) URL: <https://eps.ieee.org/publications/enews/92-publications/enews/july-2022/900>.
- [21] P. Gromala, A. Inamdar, W.D. van Driel, G.Q. Zhang, C. Bailey, L. Nguyen, B. Chan, J.E. Ryu, F. Rezaie, A. Detosky, Digital twins for electronics packaging and systems, *IEEE EPS Newsl.* November 2023 (2023) URL: <https://eps.ieee.org/publications/enews/november-2023/1070>.
- [22] H. Moeller, A. Inamdar, W.D. van Driel, J. Bredberg, P. Hille, H. Knoll, B. Vanvelde, Digital twin technology in electronics, in: W.D. van Driel, K. Pressel, M. Soyuturk (Eds.), *Recent Advances in the Reliability Assessment of Electronic Devices*, 2024.
- [23] A. Inamdar, M.V. Soestbergen, A. Mavinkurve, W.D. van Driel, G.Q. Zhang, A continuously updated package-degradation model reflecting thermomechanical changes at different thermo-oxidative stages of moulding compound, in: 24th International Conference on Thermal, Mechanical and Multi-Physics Simulation and Experiments in Microelectronics and Microsystems, EuroSimE 2023, Institute of Electrical and Electronics Engineers Inc., 2023, <http://dx.doi.org/10.1109/EUROSIME56861.2023.10100833>.
- [24] M.C. Celina, A.R. Dayile, A. Quintana, A perspective on the inherent oxidation sensitivity of epoxy materials, *Polymer* 54 (13) (2013) 3290–3296, <http://dx.doi.org/10.1016/J.POLYMER.2013.04.042>.
- [25] M.C. Celina, A. Quintana, Oxygen diffusivity and permeation through polymers at elevated temperature, *Polymer* 150 (2018) 326–342, <http://dx.doi.org/10.1016/J.POLYMER.2018.06.047>.
- [26] A.V. Cunliffe, A. Davis, Photo-oxidation of thick polymer samples—Part II: The influence of oxygen diffusion on the natural and artificial weathering of polyolefins, *Polym. Degrad. Stab.* 4 (1) (1982) 17–37, [http://dx.doi.org/10.1016/0141-3910\(82\)90003-9](http://dx.doi.org/10.1016/0141-3910(82)90003-9).
- [27] K. Jansen, *Thermomechanical Modeling and Characterization of Polymers*, TU Delft, 2007, URL: [https://www.researchgate.net/profile/K-M-B-Jansen/publication/331683452\\_Thermomechanical\\_modelling\\_and\\_characterisation\\_of\\_polymers\\_version/links/5c87bbf6458515b59e4679e1/Thermomechanical-modelling-and-characterisation-of-polymers-version.pdf](https://www.researchgate.net/profile/K-M-B-Jansen/publication/331683452_Thermomechanical_modelling_and_characterisation_of_polymers_version/links/5c87bbf6458515b59e4679e1/Thermomechanical-modelling-and-characterisation-of-polymers-version.pdf).

- [28] A. Lukichev, Physical meaning of the stretched exponential Kohlrausch function, *Phys. Lett. A* 383 (24) (2019) 2983–2987, <http://dx.doi.org/10.1016/J.PHYSLETA.2019.06.029>.
- [29] T.W. Clyne, Residual stresses in surface coatings and their effects on interfacial debonding, *Key Eng. Mater.* 116–117 (1995) 307–330, <http://dx.doi.org/10.4028/WWW.SCIENTIFIC.NET/KEM.116-117.307>, URL: <https://www.scientific.net/KEM.116-117.307>.
- [30] K.M. Jansen, D.J. Van Dijk, M.H. Husselman, Effect of processing conditions on shrinkage in injection molding, *Polym. Eng. Sci.* 38 (5) (1998) 838–846, <http://dx.doi.org/10.1002/PEN.10249>, URL: <https://onlinelibrary.wiley.com/doi/full/10.1002/pen.10249>.
- [31] X. Peng, J. Xu, Y. Cheng, L. Zhang, J. Yang, Y. Li, An analytical model for cure-induced deformation of composite laminates, *Polymers* 14 (14) (2022) 2903, <http://dx.doi.org/10.3390/POLYM14142903>.
- [32] M.Y. Lin, Y.J. Zeng, S.J. Hwang, M.H. Wang, H.P. Liu, C.L. Fang, Warpage and residual stress analyses of post-mold cure process of IC packages, *Int. J. Adv. Manuf. Technol.* 124 (3) (2022) 1017–1039, <http://dx.doi.org/10.1007/S00170-022-10436-4/TABLES/10>, URL: <https://link.springer.com/article/10.1007/s00170-022-10436-4>.
- [33] D.S. Choi, Y.T. Im, Prediction of shrinkage and warpage in consideration of residual stress in integrated simulation of injection molding, *Compos. Struct.* 47 (1–4) (1999) 655–665, [http://dx.doi.org/10.1016/S0263-8223\(00\)00045-3](http://dx.doi.org/10.1016/S0263-8223(00)00045-3).
- [34] C.C. Lee, C.C. Lee, C.P. Chang, Simulation methodology development of warpage estimation for epoxy molding compound under considerations of stress relaxation characteristics and curing conditions applied in semiconductor packaging, *Mater. Sci. Semicond. Process.* 145 (2022) 106637, <http://dx.doi.org/10.1016/J.MSSP.2022.106637>.
- [35] H.C. Cheng, Y.C. Liu, Warpage characterization of molded wafer for fan-out wafer-level packaging, *J. Electr. Packag., Trans. ASME* 142 (1) (2020) <http://dx.doi.org/10.1115/1.4044625/960579>, URL: <https://asmedigitalcollection.asme.org/electronicpackaging/article/142/1/011004/960579/Warpage-Characterization-of-Molded-Wafer-for-Fan>.
- [36] H.C. Cheng, Z.D. Wu, Y.C. Liu, Viscoelastic warpage modeling of fan-out wafer-level packaging during wafer-level mold cure process, *IEEE Trans. Compon. Packag. Manuf. Technol.* 10 (7) (2020) 1240–1250, <http://dx.doi.org/10.1109/TCPMT.2020.2992041>.
- [37] A.R. Adli, K.M. Jansen, Numerical investigation and experimental validation of residual stresses building up in microelectronics packaging, *Microelectr. Reliab.* 62 (2016) 26–38, <http://dx.doi.org/10.1016/J.MICROREL.2016.03.015>.
- [38] A. Rezaie Adli, Numerical Analysis and Experimental Verification of Stresses Building up in Microelectronics Packaging (Ph.D. thesis), Delft University of Technology, 2017, <http://dx.doi.org/10.4233/UUID:FC197D29-F9BD-4B0E-A4D5-485344D8D429>, URL: <https://repository.tudelft.nl/islandora/object/uuid%3Afc197d29-f9bd-4b0e-a4d5-485344d8d429>.
- [39] Y. Nawab, X. Tardif, N. Boyard, V. Sobotka, P. Casari, F. Jacquemin, Determination and modelling of the cure shrinkage of epoxy vinyl ester resin and associated composites by considering thermal gradients, *Compos. Sci. Technol.* 73 (1) (2012) 81–87, <http://dx.doi.org/10.1016/J.COMPOSITECH.2012.09.018>, URL: <https://hal.science/hal-01006724>.
- [40] L. Olivier, C. Baudet, D. Bertheau, J.C. Grandidier, M.C. Lafarie-Frenot, Development of experimental, theoretical and numerical tools for studying thermo-oxidation of CFRP composites, *Composites A* 40 (8) (2009) 1008–1016, <http://dx.doi.org/10.1016/J.COMPOSITESA.2008.04.005>.
- [41] L. Ernst, Refreshing fracture mechanics and high temperature aging of EMC, in: *Internal Presentation (NXP Semiconductors)*, 2016.
- [42] J. De Vreugd, K.M. Jansen, L.J. Ernst, C. Bohm, R. Pufall, High temperature storage influence on molding compound properties, in: *2010 11th International Conference on Thermal, Mechanical and Multi-Physics Simulation, and Experiments in Microelectronics and Microsystems, EuroSimE 2010*, 2010, <http://dx.doi.org/10.1109/ESIME.2010.5464541>.
- [43] J. De Vreugd, A. Sánchez Monforte, K.M. Jansen, L.J. Ernst, C. Bohm, A. Kessler, H. Preu, Effect of posture and thermal aging on molding compound properties, in: *Proceedings of the Electronic Packaging Technology Conference, EPTC, 2009*, pp. 342–347, <http://dx.doi.org/10.1109/EPTC.2009.5416524>.
- [44] B. Zhang, A. Lion, M. Johlitz, L. Ernst, K.M. Jansen, D.K. Vu, L. Weiss, Modelling of thermal aging of moulding compound by using an equivalent layer assumption, in: *2017 18th International Conference on Thermal, Mechanical and Multi-Physics Simulation and Experiments in Microelectronics and Microsystems, EuroSimE 2017*, Institute of Electrical and Electronics Engineers Inc., 2017, <http://dx.doi.org/10.1109/EUROSIM.2017.7926271>.